Available online at www.sciencedirect.com
ScienceDirect
Mathematics and Computers in Simulation 76 (2007) 141–148
MATHEMATICS AND COMPUTERS IN SIMULATION
www.elsevier.com/locate/matcom

Finite element approach to modelling evolution of 3D shape memory materials

D. Roy Mahapatra, R.V.N. Melnik *

Mathematical Modeling and Computational Sciences, Wilfrid Laurier University, 75 University Avenue W, Waterloo, Ont., Canada N2L 3C5

Available online 21 January 2007

Abstract

A general finite element framework for the application to different types of phase transforming alloys and under general thermo-mechanical loadings is presented. The developed technique is exemplified on cubic to tetragonal transformations of shape memory alloys.

Keywords: Phase transformation; Microstructure; Free energy; Finite element; Dynamics

1. Introduction

The range of applications of shape memory alloys (SMAs) has continued to widen over the recent years and it now includes transducer devices and control of dynamical systems among many others. However, mathematical modelling and analysis of the dynamics of SMAs remains a challenging task, although extensive studies have been carried out over the last three decades [2–4,9,13]. The underlying reason for that is the inherent thermo-mechanical coupling, the diffusionless transformation between the high-temperature austenite (A) phase and the low-temperature martensite (M) phases, and the strong non-linearity that at the modelling level lead to a non-convex energy minimization problem [1]. The development of consistent mathematical models that capture most of the important features of SMAs and their numerical implementation is one of the most important and challenging problems in the field.

One of the major advantages of the model discussed in the present paper is that the requirements on mesh adaptation scheme are relaxed when we interpolate the phase field represented here by order parameters η_k. The trade-off for this advantage is that a consistent evolution criteria needs to be derived from the analytic description of the microstructure using the compatibility conditions. In this paper, we outline key possible steps to achieve this. Among other important issues, the model also describes accurately the energy wells $G(\eta)$ in the case of multivariant phase transformation (PT) with essential properties of frame-indifference and material symmetry as discussed in [7,8]. The total strain is split into elastic and transformation parts. Since the transformation part can be directly linked to the conditions of A–M and M–M compatible microstructures [4], in this way we establish a link between the atomistic and continuum description of microstructure. According to the Cauchy–Born hypothesis, the consequence of that is that the atomistic reordering without diffusion and the resulting free energy $G(\eta)$ based on Born–Oppenheimer approximation becomes equivalent to the free energy or to $G(F)$, where F is the deformation gradient. The order parameters, therefore, describe

* Corresponding author. Tel.: +1 519 884 1970 3662; fax: +1 519 884 9738.
E-mail address: rmelnik@wlu.ca (R.V.N. Melnik).

0378-4754/$32.00 © 2007 IMAC. Published by Elsevier B.V. All rights reserved.
doi:10.1016/j.matcom.2007.01.014

in this approach the phenomenological link between the above two dynamics. This approach deviates from the notion of phase fractions [5] and gives a consistent framework for microstructure evolution in multivariant situation. The resulting problem becomes very challenging and up to date there is no robust mathematical model with well-defined computational steps for its solution that can deal with general dynamics of SMA over a range of deformation, stress and temperature.

2. Gibbs free energy model

Let us denote the variants of Martensite by M_k, $k = 1, \ldots, N$, where N is the number of variants. In order to model realistic situations and macroscopic samples of SMA, it is essential to incorporate the effects of the following: (1) martensitic variants (M_k); (2) thermal strain; (3) unequal compliances across the interfaces and the resulting inhomogeneity. We assume the same order of variation in the compliance tensor and the thermal expansion tensor due to transformation-induced inhomogeneity and softening. Following [11] and references therein, the Gibbs free energy density is then expressed as

$$G(\eta) = -\frac{1}{2}\boldsymbol{\sigma} : \left[\boldsymbol{\lambda}_0 + \sum_{k=1}^{N}(\boldsymbol{\lambda}_k - \boldsymbol{\lambda}_0)\varphi(\eta_k)\right] : \boldsymbol{\sigma} - \boldsymbol{\sigma} : \sum_{k=1}^{N}\boldsymbol{\varepsilon}_{tk}\varphi(\eta_k) - \boldsymbol{\sigma} : \left[\boldsymbol{\varepsilon}_{\theta 0} + \sum_{k=1}^{N}(\boldsymbol{\varepsilon}_{\theta k} - \boldsymbol{\varepsilon}_{\theta 0})\varphi(\eta_k)\right] + \sum_{k=1}^{N} f(\theta, \eta_k) + \sum_{i=1}^{N-1}\sum_{j=i+1}^{N}\bar{F}_{ij}(\eta_i, \eta_j), \tag{1}$$

where $\boldsymbol{\lambda}$ is the second-order fourth-rank compliance tensor ($\boldsymbol{\lambda}_0$ is for A phase), $\boldsymbol{\varepsilon}_{\theta 0} = \boldsymbol{\alpha}_0(\theta - \theta_\mathrm{e})$, $\boldsymbol{\varepsilon}_{\theta k} = \boldsymbol{\alpha}_k(\theta - \theta_\mathrm{e})$, $\boldsymbol{\alpha}_0$ and $\boldsymbol{\alpha}_k$ are the thermal expansion tensor of A and M_k. The function $\bar{F}_{ij}$ is the interaction potential required to preserve the frame-invariance of G with respect to the point group of symmetry and uniqueness of the multivariant PT at a given material point. The description of PT can now be generalized with three sets of order parameters: $\bar{0} = \{0, \eta_k = 0, 0\}$, $\bar{1} = \{0, \eta_k = 1, 0\}$ and $\bar{\eta}_k = \{0, \eta_k, 0\}$. The extremum property of the free energy density requires that

$$\frac{\partial G}{\partial \eta_k} = G_0\eta_k(\eta_k - 1)(\eta_k - \eta_k^b) = 0; \quad \bar{\eta}_k = \bar{0}, \bar{1}, \tag{2}$$

$$\frac{\partial^2 G}{\partial \eta_k^2} \leq 0, \quad \bar{\eta}_k = \bar{0} \quad (\mathrm{A} \to \mathrm{M}_k), \tag{3}$$

$$\frac{\partial^2 G}{\partial \eta_k^2} \leq 0, \quad \bar{\eta}_k = \bar{1} \quad (\mathrm{M}_k \to \mathrm{A}), \tag{4}$$

so that the roots $\eta_k = 0, 1$ correspond to the extrema and the root $\eta_k = \eta_k^b(\boldsymbol{\sigma}, \theta)$ represents the $\mathrm{A} \leftrightarrow \mathrm{M}$ PT barrier. Here G_0 is a scaling factor which is generally independent of stress but can depend on temperature. This argument is to leave the scope to experimentally characterize G_0 based on the fact that the stress hysteresis in metals and alloys are independent of temperature. However G_0 may be used to accommodate other sources of inelasticity, such as dislocation, although this issue is not addressed in the present work.

The transformation energy associated with $\mathrm{A} \leftrightarrow \mathrm{M}_k$ is

$$G(\boldsymbol{\sigma}, \theta, \bar{0}) - G(\boldsymbol{\sigma}, \theta, \bar{1}) = \boldsymbol{\sigma} : \boldsymbol{\varepsilon}_{tk} - \Delta G^\theta, \tag{5}$$

where ΔG^θ is the difference between the thermal parts of the Gibbs free energy density of the M and A phases, which can be obtained indirectly from experiments through the relation [6]:

$$\Delta G^\theta = -\Delta s_\mathrm{e}(\theta - \theta_\mathrm{e}) - \Delta c\theta\left[\ln\left(\frac{\theta}{\theta_\mathrm{e}}\right) - 1\right] - \Delta c\theta_\mathrm{e}, \tag{6}$$

where Δc is the difference between the specific heat of the phases, Δs_e is the jump in the specific entropy at the equilibrium temperature (θ_e). Combining Eqs. (2) and (5) after certain algebraic steps, the transformation barrier η_k^b

for the kth martensitic variant is obtained as

$$\eta_k^b = \frac{1}{G_0}\left[-6\boldsymbol{\sigma} : \boldsymbol{\varepsilon}_{tk} - 3\boldsymbol{\sigma} : (\boldsymbol{\lambda}_k - \boldsymbol{\lambda}_0) : \boldsymbol{\sigma} - 6\boldsymbol{\sigma} : (\boldsymbol{\varepsilon}_{\theta k} - \boldsymbol{\varepsilon}_{\theta 0}) + 6\Delta G^{\theta}\right] + \frac{1}{2}. \tag{7}$$

Following the steps given in [8], we arrive at the frame-invariance as well as symmetry preserving polynomial structure of the interaction potential:

$$\bar{F}_{ij} = \eta_i\eta_j(1-\eta_i-\eta_j)[B\{(\eta_i-\eta_j)^2 - \eta_i - \eta_j\} + D\eta_i\eta_j] + \eta_i^2\eta_j^2(\eta_i Z_{ij} + \eta_j Z_{ji}), \tag{8}$$

where B, D are material constants. The parameter Z_{ij} can be obtained by imposing the uniqueness property of G at a material point lying outside of the habit plan.

Note that the energy density is represented in the stress–temperature space that allows us to avoid the direct use of the deformation gradient associated with the phase transformation. As a result, following an observation made in [8], it is convenient to carry out the analysis in stress space without addressing explicitly the stress–strain hysteresis. On the other hand, if the atomic reordering during transformations is expressed in terms of continuum deformation gradient $\boldsymbol{F} = \nabla \boldsymbol{y}(\boldsymbol{x})$, then the associated large strain for the two equivalent models can be given by

$$\frac{1}{2}(\boldsymbol{F}^{\mathrm{T}}\boldsymbol{F} - \boldsymbol{I}) = -\frac{\partial G(\eta)}{\partial \boldsymbol{\sigma}} = \boldsymbol{\varepsilon}_{\mathrm{elt}} + \sum_k \boldsymbol{\varepsilon}_{tk}\varphi(\eta_k), \tag{9}$$

where $\boldsymbol{\varepsilon}_{\mathrm{elt}}$ is the elastic part of the total strain from Eq. (1). For a compatible microstructure that minimizes $G(\boldsymbol{F}) \in \mathcal{K}$ at the austenitic well, where $\mathcal{K}$ is the sequence of energy wells, it follows from the Cauchy–Born hypothesis that

$$\hat{\boldsymbol{e}}^m = \boldsymbol{F}^m \boldsymbol{U}_{\mathrm{m}} \boldsymbol{F}^a \hat{\boldsymbol{e}}^o, \tag{10}$$

where $\boldsymbol{U}_{\mathrm{m}}$ is the Bain matrix or the transformation matrix [4], $\hat{\boldsymbol{e}}^m$ and $\hat{\boldsymbol{e}}^o$ are the lattice vectors for the mth variant of M and the undeformed A lattice vector, respectively. Under zero stress, $\boldsymbol{F}^m = \boldsymbol{F}^a = \boldsymbol{R}$ is a rigid rotation.

3. Variational framework

The unknown variables in the proposed finite element formulation will be the displacements, temperature, and the order parameters η_k, $k = 1, \ldots, N$. The displacements are related to the strain $\boldsymbol{\varepsilon}$ via the standard strain–displacement relation, while the stress is given by

$$\boldsymbol{\sigma} = \left[\boldsymbol{\lambda}_0 + \sum_{k=1}^{N}(\boldsymbol{\lambda}_k - \boldsymbol{\lambda}_0)\varphi(\eta_k)\right]^{-1}\left[\boldsymbol{\varepsilon} - \sum_{k=1}^{N}\boldsymbol{\varepsilon}_{tk}\varphi(\eta_k) - \boldsymbol{\varepsilon}_{\theta 0} - \sum_{k=1}^{N}(\boldsymbol{\varepsilon}_{\theta k} - \boldsymbol{\varepsilon}_{\theta 0})\varphi(\eta_k)\right]. \tag{11}$$

In the present analysis the Green–Lagrange strain is reduced to its linear form. The phase transformation kinetics is governed by the Ginzburg–Landau equation:

$$\frac{\partial \eta_k}{\partial t} = -\sum_{p=1}^{N} L_{kp}\left[\frac{\partial G}{\partial \eta_p} + \boldsymbol{\beta}_p : \nabla\nabla\eta_p\right] + \theta_k, \tag{12}$$

where L_{kp} are positive definite kinetic coefficients, $\boldsymbol{\beta}_p$ are positive definite second rank tensor. The variable θ_k is the thermal fluctuation satisfying the dissipation–fluctuation theorem arising in context of non-equilibrium thermodynamics. Eq. (12) is complemented by the macroscopic energy conservation law:

$$\frac{\partial}{\partial t}\left[\mathcal{W} - \theta\frac{\partial \mathcal{W}}{\partial \theta}\right] - \nabla\cdot(\boldsymbol{\sigma}\cdot\dot{\boldsymbol{u}} - \boldsymbol{q}) = h_\theta, \tag{13}$$

and the momentum balance equation:

$$\rho\frac{\partial^2 \boldsymbol{u}}{\partial t^2} = \nabla\cdot\boldsymbol{\sigma} + \boldsymbol{p}, \tag{14}$$

where $\mathcal{W}$ is the Helmoltz free energy given by

$$\mathcal{W} = G + c_v\theta + \frac{1}{2}\boldsymbol{\sigma} : \left[\boldsymbol{\lambda}_0 + \sum_{k=1}^{N}(\boldsymbol{\lambda}_k - \boldsymbol{\lambda}_0)\varphi(\eta_k)\right] : \boldsymbol{\sigma} + \boldsymbol{\sigma} : \left[\boldsymbol{\varepsilon}_{\theta 0} + \sum_{k=1}^{N}(\boldsymbol{\varepsilon}_{\theta k} - \boldsymbol{\varepsilon}_{\theta 0})\varphi(\eta_k)\right], \tag{15}$$

and

$$\boldsymbol{q} = -\kappa\nabla\theta - \alpha'\kappa\nabla\frac{\partial\theta}{\partial t}, \tag{16}$$

is the heat flux approximated from the solution of the 3D Cattaneo–Vernotte equation [13], h_θ and $\boldsymbol{p}$ are the thermal loading and body force, respectively.

3.1. Spatial discretization

We interpolate the fields $\boldsymbol{u}(x, y, z, t)$, $\theta(x, y, z, t)$ and $\eta_k(x, y, z, t)$ over the domain of interest, denoted by $\Omega(x, y, z) \subset R^3$, using non-conforming finite elements with h-refinement. In the context of SMA, a similar scheme has been applied previously in [10]. Having the highest order of spatial derivatives in the governing equations as two, we choose the standard Lagrangian isoparametric interpolation function $\boldsymbol{N}$,

$$\{u_1 \quad u_2 \quad u_3\}^{\mathrm{T}} = \boldsymbol{N}_u\boldsymbol{v}^e, \qquad \theta = \boldsymbol{N}_\theta\boldsymbol{v}^e, \qquad \eta = \boldsymbol{N}_\eta\boldsymbol{v}^e, \tag{17}$$

$$\boldsymbol{v} = \{u_1 \quad u_2 \quad u_3 \quad \theta \quad \eta_1, \ldots, \eta_n\}^{\mathrm{T}}. \tag{18}$$

Here, the superscript e indicates element nodal quantities. Introducing admissible weights $\{\bar{u}_i, \bar{\theta}, \bar{\eta}_k\} \in H^{1,2}$ chosen from the linear span of $\boldsymbol{v}^e$, the variational formulation of the problem can be stated as follows:

$$\delta\Pi = \delta\Pi_{\mathrm{PT}} + \delta\Pi_\theta + \delta\Pi_u + \delta W = 0, \quad t \in [0, +\infty], \tag{19}$$

where

$$\delta\Pi_{\mathrm{PT}} = \int_\Omega \sum_{k=1}^{n}\delta\bar{\eta}_k\left[\frac{\partial\eta_k}{\partial t} - \theta_k\right]\mathrm{d}\boldsymbol{x} + \int_\Omega \sum_{k=1}^{n}\sum_{p=1}^{n}\delta\bar{\eta}_k\left[L_{kp}\left(\frac{\partial G}{\partial\eta_p} + \boldsymbol{\beta}_p : \nabla\nabla\eta_p\right)\right]\mathrm{d}\boldsymbol{x}$$
$$- \int_\Gamma \sum_{k=1}^{n}\sum_{p=1}^{n}\delta\bar{\eta}_k L_{kp}\frac{\partial G}{\partial\eta_k}\mathrm{d}s(\boldsymbol{x}), \tag{20}$$

$$\delta\Pi_\theta = \int_\Omega \delta\bar{\theta}\left[\frac{\partial}{\partial t}\left(W - \theta\frac{\partial W}{\partial\theta}\right) - \nabla\cdot(\boldsymbol{\sigma}\cdot\dot{\boldsymbol{u}})\right]\mathrm{d}\boldsymbol{x} + \int_\Omega \delta\bar{\theta}\left[\nabla\cdot\left(-\kappa\nabla\theta - \alpha'\kappa\nabla\frac{\partial\theta}{\partial t}\right)\right]\mathrm{d}\boldsymbol{x} - \int_\Gamma \delta\bar{\theta}\boldsymbol{q}_\perp\,\mathrm{d}s(\boldsymbol{x}), \tag{21}$$

$$\delta\Pi_u = \int_\Omega \delta\bar{\boldsymbol{u}}^{\mathrm{T}}\left[\rho\frac{\partial^2\boldsymbol{u}}{\partial t^2} - \nabla\cdot\boldsymbol{\sigma}\right]\mathrm{d}\boldsymbol{x} - \int_\Gamma \delta\bar{\boldsymbol{u}}^{\mathrm{T}}\boldsymbol{\sigma}_\perp\mathrm{d}s(\boldsymbol{x}), \tag{22}$$

and W is the external work done over the sample. Integrating Eqs. (19)–(22) by parts and applying divergence theorem, we obtain the discrete Euler–Lagrange form for the non-linear finite element model, which can be expressed in matrix notations as

$$\{\delta\boldsymbol{u}\}^e : \quad \int_\Omega [\boldsymbol{N}_u]^{\mathrm{T}}\rho[\boldsymbol{N}_u]\{\ddot{\boldsymbol{v}}\}^e + \int_\Omega [\boldsymbol{B}_u]^{\mathrm{T}}\{\boldsymbol{\sigma}\} = \int_\Gamma [\boldsymbol{N}_u]^{\mathrm{T}}\{\boldsymbol{p}\} + \{\boldsymbol{f}\}^e, \tag{23}$$

$$\{\delta\theta\}^e : \quad \int_\Omega [\boldsymbol{N}_\theta]^{\mathrm{T}}\rho[\dot{\boldsymbol{G}}']\{\boldsymbol{v}\}^e + \int_\Omega [\boldsymbol{N}_\theta]^{\mathrm{T}}\rho[\boldsymbol{G}']\{\dot{\boldsymbol{v}}\}^e - \int_\Omega [\boldsymbol{N}_\theta]^{\mathrm{T}}\rho[\boldsymbol{N}_\theta]\{\boldsymbol{v}\}^e([\nabla_\theta\dot{\boldsymbol{G}}']\{\boldsymbol{v}\}^e + [\nabla_\theta\boldsymbol{G}']\{\dot{\boldsymbol{v}}\}^e)$$
$$+ \int_\Omega [\boldsymbol{N}_\theta]^{\mathrm{T}}\{\boldsymbol{\sigma}\}^{\mathrm{T}}[\nabla\boldsymbol{N}_u]\{\boldsymbol{v}\}^e + \int_\Omega [\boldsymbol{B}_\theta]^{\mathrm{T}}\kappa[\boldsymbol{B}_\theta]\{\boldsymbol{v}\}^e + \int_\Omega [\boldsymbol{B}_\theta]^{\mathrm{T}}\alpha'\kappa[\boldsymbol{B}_\theta]\{\dot{\boldsymbol{v}}\}^e = \int_\Gamma [\boldsymbol{N}_\theta]^{\mathrm{T}}\{\boldsymbol{q}_\theta\}^e, \tag{24}$$

$$\{\delta\boldsymbol{\eta}\}: \quad \int_{\Omega}[\boldsymbol{N}_{\eta}]^{\mathrm{T}}[\boldsymbol{N}_{\eta}]\{\dot{\boldsymbol{v}}\}^{e}+\int_{\Omega}[\boldsymbol{N}_{\eta}]^{\mathrm{T}}[\boldsymbol{L}][\boldsymbol{G}'']\{\boldsymbol{N}_{\eta}\}\{\boldsymbol{v}\}^{e}-\int_{\Omega}[\nabla\boldsymbol{N}_{\eta}]^{\mathrm{T}}[\boldsymbol{L}][\boldsymbol{\beta}][\nabla\boldsymbol{N}_{\eta}]\{\boldsymbol{v}\}^{e}$$
$$+\int_{\Gamma}[\boldsymbol{N}_{\eta}]^{\mathrm{T}}[\boldsymbol{L}][\boldsymbol{\beta}][\nabla\boldsymbol{N}_{\eta}]\{\boldsymbol{v}\}^{e}=\int_{\Gamma}[\boldsymbol{N}_{\eta}]^{\mathrm{T}}\{\theta_{k}\}^{e}, \tag{25}$$

where $[\boldsymbol{B}_u]$ is the strain–displacement matrix and $[\boldsymbol{B}_\theta]$ is its thermal analog. The stress vector is expressed as

$$\{\boldsymbol{\sigma}\}=[\boldsymbol{C}(\eta_k)][\boldsymbol{B}_u]\{\boldsymbol{v}\}^{e}-[\boldsymbol{C}^{t}(\eta_k,\boldsymbol{\varepsilon}_{tk})][\boldsymbol{N}_{\eta}]\{\boldsymbol{v}\}^{e}-[\boldsymbol{C}^{\alpha}(\eta_k,\alpha_0,\alpha_k)][\boldsymbol{N}_{\theta}]\left(\{\boldsymbol{v}\}^{e}-[\boldsymbol{I}]\{\theta_{\mathrm{e}}\}\right), \tag{26}$$

where the elastic stiffness includes the phase inhomogeneity:

$$[\boldsymbol{C}(\eta_k)]=\left[[\boldsymbol{\lambda}_0]+\sum_{k}([\boldsymbol{\lambda}_k]-[\boldsymbol{\lambda}_0])\,\varphi(\eta_k)\right]^{-1}, \tag{27}$$

the transformation-induced stress coefficient matrix is defined as

$$[\boldsymbol{C}^{t}(\eta_k,\boldsymbol{\varepsilon}_{tk})]=[\boldsymbol{C}(\eta_k)]\sum_{k}\{\boldsymbol{\varepsilon}_{tk}\}\bar{\varphi}(\eta_k), \tag{28}$$

$$\bar{\varphi}_k=(\varphi_k/\eta_k,0), \quad |\eta_k|\geq 0, \tag{29}$$

and the temperature-induced stress coefficient matrix includes the phase inhomogeneity

$$[\boldsymbol{C}^{\alpha}(\eta_k,\alpha_0,\alpha_k)]=[\boldsymbol{C}(\eta_k)]\left([\alpha_0]+\sum_{k}([\alpha_k]-[\alpha_0])\varphi(\eta_k)\right). \tag{30}$$

The non-linear terms are decomposed as

$$G=\sum_{k}(\bar{G}_k+\bar{F}_k)\eta_k=([\bar{G}]+[\bar{F}])[\boldsymbol{N}_{\eta}]\{\boldsymbol{v}\}^{e}=[G']\{\boldsymbol{v}\}^{e}, \tag{31}$$

$$\left\{\frac{\partial G}{\eta_p}\right\}=[\tilde{G}]\{\eta\}=[G'']\{\boldsymbol{v}\}^{e}. \tag{32}$$

In Eq. (23), $\{\boldsymbol{f}\}^{e}$ is the nodal force vector. In Eq. (24), $\{\boldsymbol{q}_\theta\}^{e}$ is the thermal flux vector. Considering the effect of ambient environment surrounding the SMA sample, the total thermal flux normal to the material surface (Γ) is defined as $q_\theta=q_0-h_{\mathrm{c}}(\theta-\theta_0)$, where q_0 is the externally applied flux, θ_0 is the ambient temperature and h_{c} is the associated convection coefficient.

4. Computational scheme

We have implemented the finite element model formalized by Eqs. (23)–(26) with the associated general boundary and initial conditions in a general 3D finite element code. In what follows we concentrate on cubic to tetragonal transformations where we have to deal with three different phases so that $N=3$. We employ 8-node, 7 d.o.f/node tetrahedral element with tri-linear isoparametric interpolation and reduced Gauss-quadrature integration for shear terms. For the time integration, Newmark's scheme is employed. The analysis of stability of the resulting scheme is not trivial. Here, we note only that in the context of viscoplasticity such issues were addressed in [14] for a first-order accurate integrator. Since solid–solid phase transformations involve rates that vary over a wide range, an extension of such analysis to higher-order schemes is desirable.

Since the energy minimization process can take a different and unphysical path, a special care should be taken in organizing non-linear iterations. In particular, the phase transformation conditions in Eqs. (3) and (4) need to be enforced in a consistent manner in the incremental algorithm. The implemented algorithm can be presented in the following schematic manner:

(1) With the known matrices and vectors obtained from the time step $t = t_i$, compute the stress and transformation barrier.
(2) Check the loss of stability $A \leftrightarrow \mathrm{M}_k$ for all k. Obtain the increment $\Delta\eta_k$ by satisfying consistency condition in the neighborhood of the transformation surface (similar to the return mapping algorithm for elasto-plasticity [14]).
(3) Compute the consistent tangent matrix $[\boldsymbol{K}]_\mathrm{t}$. Here the effective internal force vector has three parts:

$$\{\boldsymbol{b}\} = \{\{\boldsymbol{f}\}_u^\mathrm{T} \quad \{\boldsymbol{f}\}_\theta^\mathrm{T} \quad \{\boldsymbol{f}\}_\eta^\mathrm{T}\}^\mathrm{T}, \quad \boldsymbol{f}_u = \frac{\partial \Pi_u}{\partial \boldsymbol{u}}, \quad \boldsymbol{f}_\theta = \frac{\partial \Pi_\theta}{\partial \theta}, \quad \boldsymbol{f}_\eta = \frac{\partial \Pi_\mathrm{PT}}{\partial \eta_k}.$$

The incremental update at nth iteration is obtained as

$$\{\Delta \boldsymbol{v}\}_{n+1}^e = -[\boldsymbol{K}]_\mathrm{t}^{-1} \left(\{\boldsymbol{b}\}_{n+1}^\mathrm{int} - \{\boldsymbol{b}\}_{n+1}^\mathrm{ext} \right), \tag{33}$$

$$[\boldsymbol{K}]_\mathrm{t} = \bigcup_e \frac{\partial \boldsymbol{b}}{\partial \boldsymbol{v}^e},$$

(4) Solve Eq. (33) by Newton iterations until a specified convergence is achieved.
(5) Compute the updated vectors, velocity and acceleration and move to the next time step $t_{i+1} = t_i + \Delta t$.

4.1. Error estimate

The quantities of interest include $\boldsymbol{\varepsilon}$, $\boldsymbol{\eta}$, $\boldsymbol{\sigma}$, and θ. Following the analysis presented in [12], it can be observed that we have a similar form of differential-difference equation in all those cases where the original problem can be reduced to 1D. The main difference is related to the phase kinetics, a process that evolves on a much faster time scale than that of the thermodynamics. In this case, it is the $\nabla\eta$ that is of importance as it is responsible for sharp interfaces and microstructures. The following quantity, defined in a way analogous to that of [12] using energy arguments, can be used for the analysis of the convergence properties of the constructed scheme:

$$E_1 = \rho^{-1}\kappa\theta_0\|\boldsymbol{\varepsilon}\|^2 + \|\dot{\boldsymbol{u}}\|^2 + (c_v + \kappa)\|\theta\|^2 + \|(\nabla\eta)\|^2. \tag{34}$$

As an example, the function E_1, plotted as a function of time for the problem discussed in the next section, is presented in Fig. 1 (a). In Fig. 1(b) the same plot is presented on the logarithmic scale.

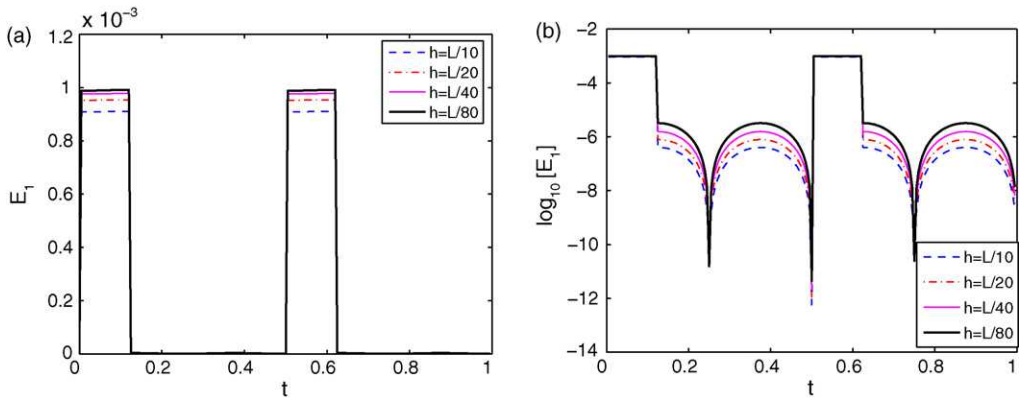

Fig. 1. Time evolution of the energy-based quantity E_1.

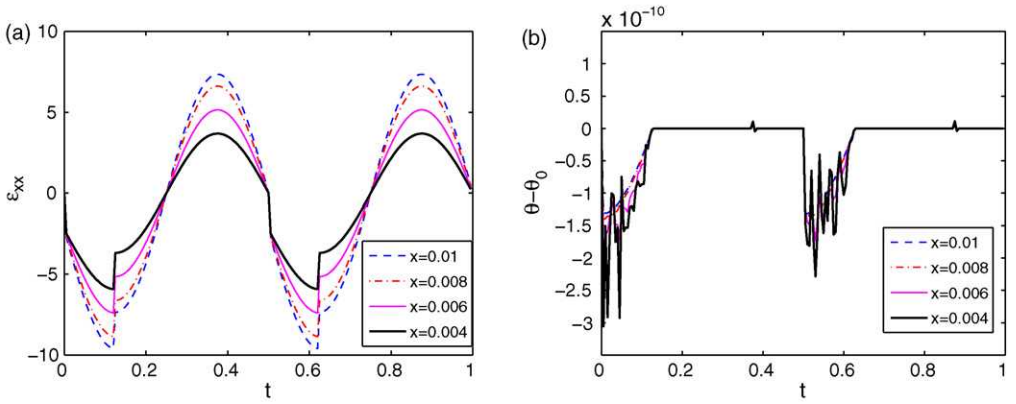

Fig. 2. (a) Strain evolution and (b) stress-induced thermal fluctuations.

5. Numerical simulation

Based on the developed methodology, we have analyzed stress-induced transformations under in-plane longitudinal harmonic stress $\sigma_{xx}(y, t) = \sigma_0 \sin(2\pi ft)$, $\sigma_0 = 160$ MPa where $f = 2$ Hz has been applied at one edge of a 100 mm × 50 mm × 100 μm Ni–Al film. Dirichlet boundary condition has been applied at $x = 0$. The film has been stressed at the edge $x = L = 100$ mm. The surfaces are assumed to be in ambient environment ($\theta = 298$ K), $\theta_e = 215$ K. Fig. 2 shows the A–M transformation during periodic loading where the kinks in the strain history (Fig. 2(a)) indicate the formation of martensite accompanied by the corresponding drop in temperature (Fig. 2(b)).

6. Conclusions

A finite element approach based on a new Landau–Ginzburg free energy model for multivariant martensitic phase transformation has been reported. It is shown that at the onset of phase transformation, the phase field can be uniquely identified from the conditions of microstructural compatibility. While doing so, the main advantage in the context of solving a discrete version of the energy minimization problem is that the finite element mesh needs not be adapted by tracking the A–M_k or M_k–M_j interfaces. Instead, the order parameters (η_k) can be updated from the equivalent deformation gradient in a point-wise sense. A computational scheme has been developed, based on which the quantities interest can be simulated with desired accuracy. Numerical studies on the convergence of one of such quantities of interest in strain–temperature space are carried out under uniform h-refinement scheme. The results demonstrate good performance of the computational scheme in capturing the stress-induced phase transformation.

References

[1] J.M. Ball, Some open problems in elasticity, in: Geometry, Mechanics and Dynamics, Springer, New York, 2002, pp. 3–59.
[2] J.M. Ball, C. Cartensen, Compatibility conditions for microstructures and the austenite–martensite transition, Mater. Sci. Eng. A 273 (1999) 231–236.
[3] P. Belik, M. Luskin, A computational model for the indentation and phase transition of a martensitic thin film, J. Mech. Phys. Solids 50 (2002) 1789–1815.
[4] K. Bhattacharya, Microstructure of Martensite, Oxford University Press, 2003.
[5] J.G. Boyd, D.C. Lagoudas, A thermodynamical constitutive model for shape memory materials. Part I. The monolithic shape memory alloy, Int. J. Plasticity 12 (6) (1996) 805–842.
[6] S. Fu, Y. Huo, I. Muller, Thermodynamics of pseudoelasticity—an analytical approach, Acta Mech. 99 (1991) 1–19.
[7] V.I. Levitas, D.L. Preston, Three-dimensional Landau theory for multivariant stress-induced martensitic phase transformations. I. Austenite ↔ martensite, Phys. Rev. B 66 (2002) 134206.
[8] V.I. Levitas, D.L. Preston, Three-dimensional Landau theory for multivariant stress-induced martensitic phase transformations. II. Multivariant phase transformations and stress space analysis, Phys. Rev. B 66 (2002) 134207.
[9] V.I. Levitas, D.L. Preston, Three-dimensional Landau theory for multivariant stress-induced martensitic phase transformations. III. Alternative potentials, critical nuclei, kink solutions, and dislocation theory, Phys. Rev. B 68 (2003) 134201.

[10] B. Li, M. Luskin, Finite element analysis of microstructure for the cubic to tetragonal transformation, SIAM J. Numer. Anal. 35 (1998) 376–392.
[11] D.R. Mahapatra, R.V.N. Melnik, A Dynamic Model for Phase Transformations in 3D Samples of Shape Memory Alloys, vol. 3516, LNCS Springer-Verlag, 2005, pp. 25–32.
[12] P. Matus, R.V.N. Melnik, L. Wang, I. Rybak, Application of fully conservative schemes in nonlinear thermoelasticity: modelling shape memory materials, Math. Comput. Simul. 65 (2004) 489–510.
[13] R.V.N. Melnik, A.J. Roberts, K.A. Thomas, Computing dynamics of copper-based shape memory alloys via center manifold reduction of 3D models, Comput. Mater. Sci. 18 (2000) 255–268.
[14] J.C. Simo, T.J.R. Hughes, Computational Inelasticity, Springer-Verlag, 1997.